Highly nonlinear frequency-dependent spin-wave resonance excited via spin-vorticity coupling

Yuki Kurimune,[1] Mamoru Matsuo,[2,3,4,5] Sadamichi Maekawa,[4,2] and Yukio Nozaki[1,6,*]

[1]*Department of Physics, Keio University, Yokohama 223-8522, Japan*
[2]*Kavli Institute for Theoretical Sciences, University of Chinese Academy of Sciences, No. 3, Nanyitiao, Zhongguancun, Haidian District, Beijing 100190, China*
[3]*CAS Center for Excellence in Topological Quantum Computation, University of Chinese Academy of Sciences, Beijing 100190, China*
[4]*RIKEN Center for Emergent Matter Science (CEMS), Wako, Saitama 351-0198, Japan*
[5]*Advanced Science Research Center, Japan Atomic Energy Agency, Tokai 319-1195, Japan*
[6]*Center for Spintronics Research Network, Keio University, Yokohama 223-8522, Japan*

(Received 24 February 2020; revised 30 September 2020; accepted 14 October 2020; published 9 November 2020)

A nonuniform vorticity of lattice deformation in a surface acoustic wave (SAW) can generate a spin current (SC) in nonmagnetic metals via spin-vorticity coupling (SVC). We demonstrated a strong enhancement of SVC-derived SC generated in Cu and Pt films with increasing the frequency of the SAW by observing the spin-wave resonance (SWR) in an adjacent NiFe film. The comparative amplitudes and high-order frequency variations of SWR in NiFe/Cu and NiFe/Pt bilayers imply that the amplitude of the SC generated via SVC in a SAW is robust against the strength of spin-orbit interaction in nonmagnetic metals.

DOI: 10.1103/PhysRevB.102.174413

I. INTRODUCTION

A nonconservative flow of spin angular momentum, i.e., spin current (SC), is necessary to control the magnetization of nanoscaled ferromagnets in spintronic devices such as magnetic random access memory [1–5] and spin auto-oscillators [6–8]. A variety of methods to produce a SC and the consequent torque on magnetization have been developed, e.g., the spin Seebeck effect [9], nonlocal spin injection from ferromagnetic conductors [10], the spin pumping effect [11–14], the spin Hall effect (SHE) [15–17], and the Rashba-Edelstein effect [18,19]. All of these methods utilize ferromagnetic materials and/or nonmagnetic heavy metals with strong spin-orbit interaction (SOI), which plays an important role in SC generation via SHE. The necessity of particular materials to produce a SC reduces a degree of freedom in the material choice of spintronic devices.

Recently, an alternative method to produce a SC from a macroscopic rotational motion was theoretically proposed [20] followed by experimental demonstrations using a turbulent flow of liquid metal [21], a surface acoustic wave (SAW) in a Cu film [22], and a gradient in the electrical mobility in a surface-oxidized Cu film [23]. A nonuniform vorticity of the velocity field in the macroscopic rotation leads to a nonuniform spin accumulation via spin-vorticity coupling (SVC) [24–28], which enables a universal conversion between macroscopic and microscopic spin angular momentum according to an angular momentum conservation law. Kobayashi *et al*. demonstrated a spin-wave resonance (SWR) by injecting a SAW into a NiFe/Cu bilayer deposited on a $LiNbO_3$ substrate. The schematic principle of the SAW-driving SWR is shown in Fig. 1(a). The magnitude of vorticity of the lattice deformation in the SAW exponentially decays in the depth direction. The gradient of vorticity in the Cu layer leads to a gradient of spin accumulation via SVC which generates an alternating SC. When the SC is injected to the NiFe fabricated adjacent to Cu, a spin wave whose wave number is consistent with that of the SAW can be resonantly excited.

In this article, we experimentally demonstrated a strong enhancement of SC generation with increasing the frequency of SAW by measuring the SWR in a NiFe film attached to a Cu, Ti (weak SOI), or Pt (strong SOI) film as a SC-generating material. For comparison, the frequency dependencies of the SWR caused by the Barnett [29–32] and the magnetoelastic (ME) [33,34] effects in ferromagnetic metals (FMs) were also measured using NiFe and Ni single films, respectively, because these effects also affected the frequency dependencies of SWR in NiFe/nonmagnetic metal (NM) bilayers. We found that the SVC can generate the SC in the Cu comparable to the Pt although the strength of SOI is totally different. Moreover, from the order of the nonlinear frequency dependence of SC generation, we determined the primary contribution of SVC in the SC generation using SAW. As described in Sec. II, the theory predicts that the SVC can create spin accumulation in conductive materials in two different processes. These findings are significant to understand the microscopic mechanism of the SVC and the material dependence.

The reminder of this paper is organized as follows. Section II briefly summarizes the theory for SC generation via SVC together with the frequency-dependent expression of the SC which plays a significant role for quantitative understanding of the SVC-related SC generation. Sections III and IV describe the experimental setup and the measured SWR excited in the NiFe attached to nonmagnetic materials by applying the Rayleigh-type SAW (R-SAW), respectively. The

*Corresponding author: nozaki@phys.keio.ac.jp

 ©2020 American Physical Society

dependence of the SWR intensity on the frequency of R-SAW, the nonmagnetic materials, and the angle of external field application are discussed in Sec. V quantitatively. Finally, the paper concludes with Sec. VI.

II. THEORY FOR SPIN-CURRENT GENERATION VIA SVC

The Hamiltonian of the SVC is defined as $H_{\rm SVC} = -(\hbar/2)\boldsymbol{\sigma}\cdot(\boldsymbol{\Omega}/2)$, where $\hbar$ is the reduced Plank constant, and $\boldsymbol{\sigma}$ are the Pauli matrices [35]. The vorticity $\boldsymbol{\Omega}$ is given by $\boldsymbol{\Omega} = \nabla\times(\partial\mathbf{u}/\partial t)$, where $\mathbf{u}$ is the displacement vector. According to the SVC theory, a gradient of the vorticity leads to a spin-dependent force field which produces the SC. Moreover, collisions and relaxations between spins are also modulated by the vorticity of the macroscopic rotational motion. The consequent temporal and spatial variation in spin accumulation $\delta\mu$ is described by the spin diffusion equation [20,35]:

$$\left(\frac{\partial}{\partial t} - D\nabla^2 + \frac{1}{\tau_{\rm sf}}\right)\delta\mu = \hbar\frac{\partial\Omega^z}{\partial t} - \frac{\hbar}{\tau_{\rm sf}}\zeta\Omega^z. \tag{1}$$

D and $\tau_{\rm sf}$ are the diffusion constant and the spin-flip time modulated by SVC, respectively. The right-hand side of Eq. (1) represents two sources for spin accumulation; one is proportional to the time derivative of the vorticity, and another is proportional to the vorticity itself. These are derived from a quantum-kinetic theory, where the spin dynamics is described in terms of the nonequilibrium distribution function obeying a generalized Boltzmann equation. The distribution function is determined by two processes: (i) force fields acting on the electron spins and (ii) effects of collisions or relaxations between spins. The SC generated by processes (i) and (ii) corresponds to the first and second sources of Eq. (1), respectively. It is predicted that the SC owing to process (ii) is enhanced by the coarse graining from the microscopic to macroscopic scale. ζ is a normalization factor representing the conversion efficiency between spin and mechanical rotation.

When the R-SAW with a vorticity along the z axis is injected into an x-y semifinite NM, the distribution of the vorticity amplitude is given by [36]

$$\Omega^z = \frac{\omega^2 u_0}{c_{\rm t}} e^{-k_{\rm t}y} e^{i(kx-\omega t)}, \tag{2}$$

where ω is an angular frequency of the R-SAW, u_0 is the deformation amplitude of the R-SAW, $c_{\rm t}$ is the transverse velocity of a sound wave, and k is the longitudinal wave number. The transverse wave number $k_{\rm t}$ is given by $k_{\rm t} = k\sqrt{1-\xi^2}$, where ξ is a constant given by $\xi \approx (0.875 + 1.12\nu)/(1+\nu)$ with Poisson ratio ν [20]. Then the z-polarized alternating SC in the y direction is calculated by substituting the solution of Eq. (1) to the equation $J_{\rm s} = (\sigma_0/e)\nabla\delta\mu$ with the electric conductivity σ_0, which leads to [20,22]

$$J_{\rm s} = (\tau_{\rm sf}\omega - i\zeta)J_{\rm s}' e^{i(kx-\omega t)} \equiv \left(J_{\rm s}^{\tau_{\rm sf}} - iJ_{\rm s}^{\zeta}\right)e^{i(kx-\omega t)}, \tag{3}$$

where

$$J_{\rm s}' \approx \frac{\hbar\sigma_0\omega^3 u_0}{ec_{\rm t}^2}\left(1 + \frac{k_{\rm t}^2\lambda_{\rm s}^2}{1-\xi^2}\right)^{-1/4}\frac{\sqrt{1-\xi^2}}{\xi}\frac{y}{\lambda_{\rm s}} \tag{4}$$

for $k_{\rm t}y \ll 1$, where $\lambda_{\rm s} = \sqrt{D\tau_{\rm sf}}$ is the spin diffusion length. As seen in Eq. (3), the SC consists of two contributions. The SCs proportional to $\tau_{\rm sf}$ (denoted as $J_{\rm s}^{\tau_{\rm sf}}$) and ζ (denoted as $J_{\rm s}^{\zeta}$), respectively, are attributed to the diffused sources proportional to the time derivative of the vorticity and the vorticity itself in Eq. (1). If the former is predominant for SC generation, materials with a weak SOI (e.g., Cu and Al) are suitable for SC generation because the magnitude of SC is proportional to $\tau_{\rm sf}$. Recently, Takahashi *et al.* succeeded in generating a time-independent SC using the time-averaged vorticity in turbulent flow of liquid mercury [21], which suggests that a SC can be generated via SVC even if $\partial\Omega^z/\partial t = 0$. Moreover, Eqs. (3) and (4) clearly indicate that the intensity of the SC generated via SVC is proportional to the cubic and/or quartic of frequency. Namely, the SC amplitude is expected to show a remarkable variation in frequency and can be strongly enhanced by increasing the frequency of the vorticity.

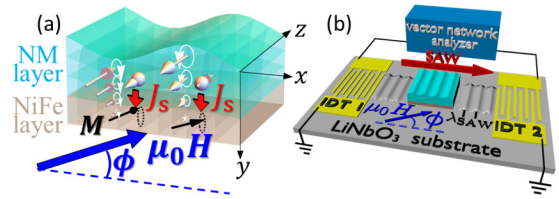

FIG. 1. (a) Schematic illustration of an SWR excited by propagating an R-SAW through a NiFe/NM bilayer. The R-SAW generates a nonuniform alternating SC via SVC in NMs. When a static magnetic field is applied at an angle ϕ from the propagation direction of the R-SAW, a spin wave is possibly excited in the NiFe layer due to the spin-transfer torque by the injected SC, the Barnett field, and/or the ME field. (b) Measurement setup for observing the SWR. The R-SAW attenuation owing to the SWR can be measured from the S_{21} signal using a vector network analyzer.

III. EXPERIMENTAL SETUP

When a static magnetic field is applied at an angle ϕ from the propagation direction of an R-SAW as shown in Fig. 1(a), a spin wave is excited via spin-transfer torque (STT) [37]. In the case of $\phi = 0$, this spin wave is regarded as a magnetostatic backward-volume wave (MSBVW) because its wave vector is consistent with the wave vector of the R-SAW parallel to the equilibrium direction of the magnetization. The microwave (MW) absorption in the NiFe/NM bilayer owing to the SWR excitation, i.e., the R-SAW attenuation, can be measured using a vector network analyzer. Note that three origins of SWR excitation are expected: the STT caused by the SVC-derived SC, the Barnett effect, and the ME effect. The effective fields of the Barnett and the ME effects are given by following equations [29,34]:

$$h_{\rm B} = \frac{\Omega^z}{2\gamma}\cos\phi = \frac{\omega^2 u_0}{2c_{\rm t}\gamma}e^{-k_{\rm t}y}\cos\phi\; e^{i(kx-\omega t)}, \tag{5}$$

$$h_{\rm ME}^{\rm IP} = \frac{2b_1}{M_{\rm s}}\varepsilon_{xx}\sin\phi\cos\phi, \quad h_{\rm ME}^{\rm OOP} = \frac{2b_2}{M_{\rm s}}\varepsilon_{xy}\cos\phi, \tag{6}$$

where γ is the gyromagnetic ratio of the FM, b_1 and b_2 are the ME coupling constants, $M_{\rm s}$ is the saturation magnetization of the FM, and ε_{xx} and ε_{xy} are the strain tensor components. From the comparison of Eqs. (3)–(6), the power order of $J_{\rm s}$ with respect to ω is much higher than those of $h_{\rm B}$, $h_{\rm ME}^{\rm IP}$, and $h_{\rm ME}^{\rm OOP}$.

Namely, we can determine the dominant contribution to the SWR among the three origins from the frequency dependence of the MW absorption.

Our experimental setup for observing an SWR in a NiFe/NM bilayer is shown in Fig. 1(b). Two interdigital transducers (IDTs) consisting of 30-nm-thick Au were fabricated on a $LiNbO_3$ piezoelectric substrate. A MW with an amplitude of -5 dBm was transmitted from the left IDT1 and was detected by the right IDT2. We used a 128° Y-cut $LiNbO_3$ substrate whose R-SAW-dispersion relation is given by $\omega = \xi c_t k$ [20]. We can vary the excitation frequency of the R-SAW by changing the structural period of the IDT which is consistent with the wavelength of the excited R-SAW. In our experiment, the R-SAW wavelengths were varied from 2.0 to 3.0 μm at intervals of 0.2 μm, and consequent R-SAW frequencies ranged from 1.3 to 1.9 GHz. A 400×400 μm^2 rectangle of bilayer consisting of NiFe (20 nm)/NM [NM = Cu (200 nm), Pt (28 nm), or Ti (200 nm)] was deposited between IDTs. The thickness of the NM was set so as to be consistent with the spin diffusion length of the NM because the magnitude of SC injected into NiFe is maximized at this condition. For comparison, devices with NiFe (20 nm) and Ni (20 nm) single layers were also fabricated to evaluate the contributions of the Barnett and the ME effects, respectively. A static magnetic field ranging from -20 to 20 mT was applied in the film plane at an angle ϕ from the propagation direction of the R-SAW. We conducted a frequency-domain evaluation of the R-SAW amplitude at a given magnetic field by measuring the S_{21} parameter using a vector network analyzer.

IV. EXPERIMENTAL RESULTS

Figure 2 shows color plots of the MW absorption as functions of frequency and magnetic field measured for NiFe and Ni single layers and NiFe/NM bilayers. The structural period of the IDT was set to 2.4 μm. The static field was applied at $\phi = 0$ for NiFe/NM and NiFe films so as to maximize the STT and Barnett field, while $\phi = \pi/4$ was chosen for a Ni film so as to maximize the mixed ME fields [33]. As shown in the Appendix, the peak intensity of the R-SAW decreases with increasing the fundamental frequency due to the increase of conductor resistance loss of the IDTs. To compensate for the difference in the conductor resistance loss among the devices, we used the reduced-MW absorption defined as [22]

$$\Delta P^{\mathrm{norm}}(f, H) = \frac{|\boldsymbol{P}_{21}(f, H) - \boldsymbol{P}_{21}(f, H_{\mathrm{ref}})|}{P_{21}(f_{\mathrm{res}}, H_{\mathrm{ref}})}. \tag{7}$$

Here, $\boldsymbol{P}_{21}(f, H)$ is the complex power of the transmitted-MW calculated from S_{21} at a given frequency f and magnetic field H. The reference magnetic field $\mu_0 H_{\mathrm{ref}} = -20$ mT is sufficient to saturate the magnetization of NiFe or Ni; thus, the field-independent signals can be removed by subtracting $\boldsymbol{P}_{21}(f, H_{\mathrm{ref}})$ from $\boldsymbol{P}_{21}(f, H)$. The subtracted P_{21} is divided by the peak intensity $P_{21}(f_{\mathrm{res}}, H_{\mathrm{ref}})$, where f_{res} is the R-SAW excitation frequency. The magnitude of the reduced-MW absorption is independent of u_0, because both the R-SAW-excitation power $P_{21}(f_{\mathrm{res}}, H_{\mathrm{ref}})$ and the MW absorption owing to the SWR, $|\boldsymbol{P}_{21}(f, H) - \boldsymbol{P}_{21}(f, H_{\mathrm{ref}})|$, are proportional to u_0^2. As shown in Fig. 2(a), large-MW absorption was observed in NiFe/Cu at $f_{\mathrm{res}} = 1.60$ GHz, where the R-SAW

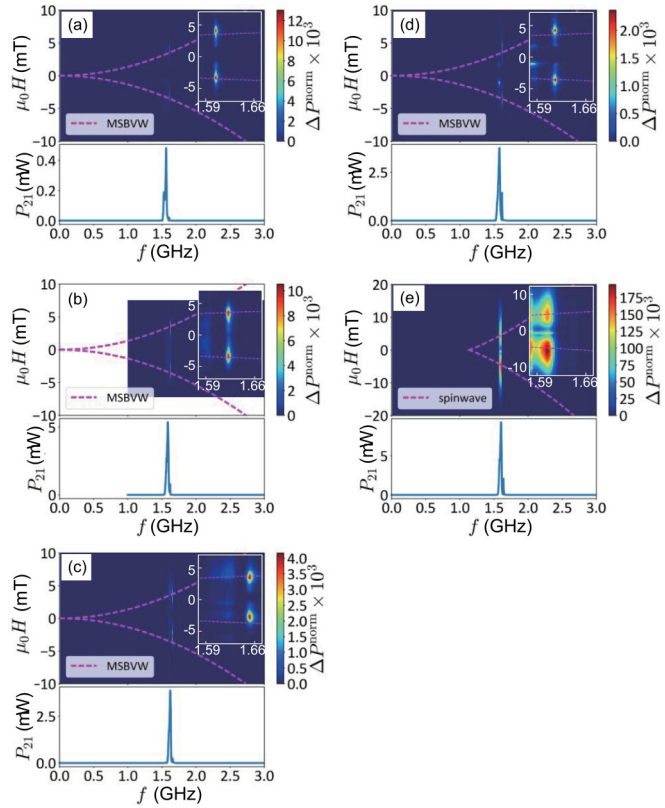

FIG. 2. Color plots of the MW absorption ΔP^{norm} as functions of frequency and magnetic field measured for (a) NiFe/Cu, (b) NiFe/Pt, and (c) NiFe/Ti bilayers, and (d) NiFe and (e) Ni single layers. The period of the IDT finger was set to 2.4 μm and the magnetic field was applied at (a–d) $\phi = 0$ and (e) $\phi = \pi/4$. The MW absorption was observed at magnetic fields where the excitation frequency of the spin wave matches the eigenfrequency of the R-SAW.

was strongly excited. The dispersion relation of the MSBVW, which is excited in the NiFe layer, is given by [38]

$$f_{\mathrm{res}} = \frac{\gamma}{2\pi}\sqrt{|H|\left(|H| + \frac{M_s}{\mu_0}\frac{1 - e^{-k_{\mathrm{sw}} d}}{k_{\mathrm{sw}} d}\right)}, \tag{8}$$

where d is the thickness of the NiFe, k_{sw} is the wave number of the MSBVW, and $M_s = 0.98$ T is the saturation magnetization of the NiFe. The dispersion relation is indicated by the magenta guidelines in Figs. 2(a)–2(d). Strong-MW absorptions were clearly observed at magnetic fields where the excitation frequency of MSBVW matches the eigenfrequency of the R-SAW.

As shown in our previous study on the SAW-induced SWR [22], the dependence of ΔP^{norm} on the angle of external magnetic field is helpful to determine the primary source of the magnetic torque which excites the SWR. In the R-SAW device schematically shown in Fig. 1, the vorticity vector is parallel to the z axis. Both the Barnett field in FMs and the spin polarization of the SC generated in the NM via SVC are, therefore, parallel to the z axis. As a consequence, the torque amplitude owing to the SC or the Barnett field will be at a maximum when the FM is magnetized along the x axis. Conversely, a torque originated from a magnetoelastic effect in the FM is enlarged when the magnetization direction

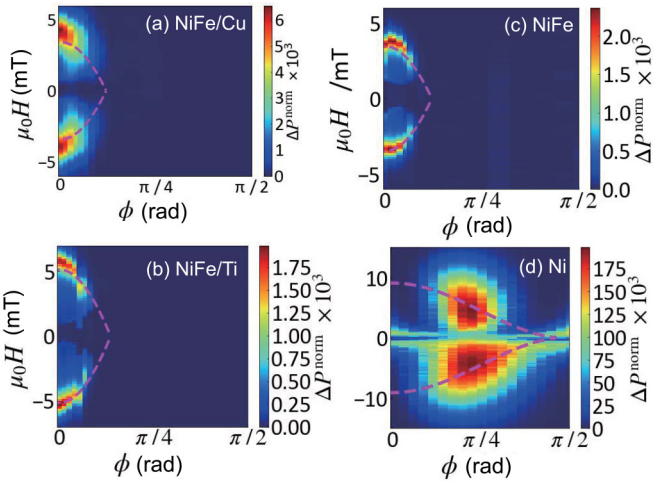

FIG. 3. Color plots of the MW absorption $\Delta P^{\rm norm}$ as functions of angle ϕ and magnitude of magnetic field measured for (a) NiFe/Cu and (b) NiFe/Ti bilayers, and (c) NiFe and (d) Ni single layers. Magenta broken lines represent the resonant condition for SWR which is given by Eqs. (9)–(11).

deviates from the x axis [33]. A propagation of the R-SAW at the FM produces both longitudinal and shear strains whose effective fields are proportional to $\sin\phi\cos\phi$ and $\cos\phi$, respectively. In the case of R-SAW, the longitudinal strain is dominated so that the effective field owing to the combined strains becomes maximum approximately at $\pi/4$ from the x axis. Figure 3 shows color plots of the MW absorption as functions of angle ϕ and magnitude of magnetic field. As shown by the magenta broken lines in Fig. 3, strong MW absorptions clearly appeared at the resonant condition for the SWR which is given by

$$f_{\rm res} = \frac{\gamma}{2\pi}\sqrt{\left(H + \frac{2A}{M_s}k^2\right)\left(H + \frac{2A}{M_s}k^2 + \frac{M_s}{\mu_0}F(k)\right)}, \quad (9)$$

where

$$F(k) = 1 - P(k)\cos^2\phi + \frac{M_s}{\mu_0(H + 2Ak^2/M_s)}P(k)(1 - P(k))\sin^2\phi \quad (10)$$

and

$$P(k) = 1 - \frac{1 - e^{-kd}}{kd}. \quad (11)$$

Figure 4 shows the angular dependence of the peak intensity of $\Delta P^{\rm norm}$. As shown in Fig. 4, when the SWR was excited in the NiFe/NM bilayer or NiFe single layer, the peak value was maximized at $\phi = 0$ followed by a monotonous decrease with ϕ. On the contrary, the strongest SWR was observed at $\phi \approx \pi/4$ in the Ni single layer. These results are consistent with the angular dependence of effective fields owing to STT, Barnett, and magnetoelastic effects. Moreover, as shown in Figs. 2 and 3, the peak intensities of $\Delta P^{\rm norm}$ at positive and negative magnetic fields are almost identical except for the Ni single layer. The nonreciprocal SWR observed in the Ni single layer is attributable to the coexistence of normal and shear strains [39]. Namely, the reciprocal properties of the SWR in

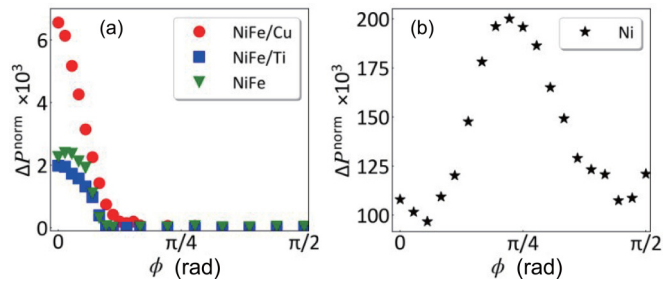

FIG. 4. Peak value of $\Delta P^{\rm norm}$ measured for (a) NiFe/NM bilayers and NiFe single layer and (b) Ni single layer as a function of angle ϕ of the external field application.

the NiFe/NM bilayer and NiFe single layer also support that the SWR is not excited by the magnetoelastic effect of the R-SAW.

As shown in Fig. 2(b), NiFe/Pt showed the MW absorption as large as NiFe/Cu, which implies that the comparable STT occurred with Cu and Pt whose SOIs are quite different. The amplitude of the SC seems to be robust against the strength of SOI in NMs. On the other hand, when highly conductive Cu in the bilayer was replaced with poorly conductive Ti, or when the NM layer adjacent to NiFe was absent, the MW absorption was suppressed significantly as shown in Figs. 2(c) and 2(d). These results suggest that the presence of the highly conductive NM layer is essential for exciting the SWR via STT in NiFe, because the SVC-derived SC is proportional to the electric conductivity of the NM as shown in Eqs. (3) and (4).

Also, the SWR intensity in a Ni film is shown in Fig. 2(e). The magenta guidelines indicate the dispersion relation of the spin wave at $\phi = \pi/4$ which supports the successful excitation of SWR by the mixed ME fields similar to the previous report [33].

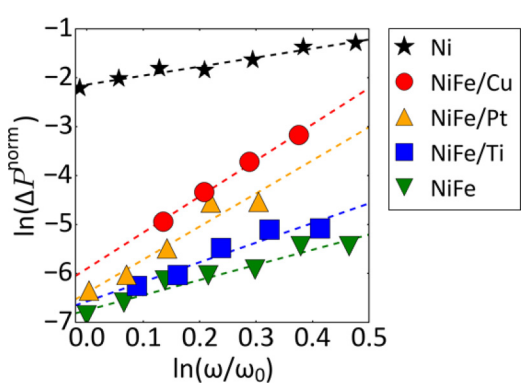

FIG. 5. R-SAW-frequency dependence of the MW absorption in NiFe/Cu, NiFe/Pt, NiFe/Ti, NiFe ($\phi = 0$) and Ni ($\phi = \pi/4$). The MW absorption in NiFe/Cu and NiFe/Pt showed higher-order changes in frequency than those in NiFe/Ti, NiFe, and Ni. The dashed lines show the results of fitting the data points with linear functions.

V. DISCUSSION

As shown in Fig. 5, we measured the frequency dependence of the MW absorption in the form of a double-logarithmic plot. In the R-SAW device, the fundamental frequency was varied in the range from 1.3 to 1.9 GHz. The lowest frequency was chosen so that the microwave absorption that appeared at positive and negative magnetic fields could be separately observed. On the other hand, the highest frequency was restricted by the difficulty in the microfabrication of the IDT. To dispel concerns that the range of frequency in Fig. 5 is insufficiently narrow to discuss the power order of frequency dependence in ΔP^{norm}, we evaluated the uncertainty in measurement by conducting three different measurements for each sample at each frequency. The magnitudes of the standard deviation evaluated from the repeated measured values of ΔP^{norm} are smaller than the size of plots in Fig. 5. Consequently, the range of frequency in Fig. 5 is sufficient to compare the frequency dependencies of ΔP^{norm} among samples. The dashed lines in Fig. 5 show the results of fitting the data points with linear functions. The gradient values of the best fit curves are 1.84 ± 0.06, 7.38 ± 0.04, 6.76 ± 0.19, 4.00 ± 0.13, and 3.09 ± 0.11 for Ni, NiFe/Cu, NiFe/Pt, NiFe/Ti, and NiFe, respectively. As seen in Fig. 2, the values of ϕ were fixed at zero for NiFe/NM and NiFe, and at $\pi/4$ for Ni. In order to quantitatively evaluate the SC generated via SVC, we calculated the power loss owing to the magnetic torques from the SC, the Barnett field, and the ME field. The magnetization dynamics is generally described by the Landau-Lifshitz-Gilbert-Slonczewski equation [37]:

$$\frac{\partial \boldsymbol{M}}{\partial t} = -\gamma[\boldsymbol{M} \times \boldsymbol{H}_{\mathrm{eff}}] + \frac{\alpha}{M}\left[\boldsymbol{M} \times \frac{\partial \boldsymbol{M}}{\partial t}\right] + \boldsymbol{\tau}_{\mathrm{STT}}, \tag{12}$$

where $\boldsymbol{M}$ is the vector of local magnetization and α is the Gilbert damping coefficient. $\boldsymbol{H}_{\mathrm{eff}}$ is the effective field given by

$$\boldsymbol{H}_{\mathrm{eff}} = \boldsymbol{H} - \overleftrightarrow{N}\frac{\boldsymbol{M}}{\mu_0} + \boldsymbol{h}_{\mathrm{B}} + \boldsymbol{h}_{\mathrm{ME}}^{\mathrm{IP}} + \boldsymbol{h}_{\mathrm{ME}}^{\mathrm{OOP}}, \tag{13}$$

which consists of the static magnetic field, the demagnetizing field, the Barnett field, and the in-plane and out-of-plane components of the ME field. The STT owing to the z-polarized SC is given by [37]

$$\boldsymbol{\tau}_{\mathrm{STT}} = -CJ_{\mathrm{s}}\big[\boldsymbol{M} \times (\boldsymbol{M} \times \boldsymbol{e}_z)\big]. \tag{14}$$

In Eq. (14), $C = \gamma\hbar g/2eM_{\mathrm{s}}^2 d$, where $g = [-4 + 3(1 + P)^3/4P^{3/2}]^{-1}$ with the spin polarization P. From the relation $P_{\mathrm{SAW}} = \omega M_{\mathrm{LNO}} W u_0^2$ [40], where $M = 1.4 \times 10^{11}$ J m^{-3} is a material constant for $LiNbO_3$ and $W = 355$ μm is the finger length of the IDT, the reduced-MW absorption is expressed as

$$\Delta P^{\mathrm{norm}} = \frac{1}{\omega M_{\mathrm{LNO}} W u_0^2}\frac{\omega}{2\pi}\int \boldsymbol{H}_{\mathrm{eff}}\, d\boldsymbol{M}. \tag{15}$$

For a small precession limit, $\boldsymbol{M}$ can be approximated as $\boldsymbol{M} \approx (M_{\mathrm{s}}, m_y e^{i\omega t}, m_z e^{i\omega t})$, where $|m_y|, |m_z| \ll M_{\mathrm{s}}$. Finally, Eq. (15) is calculated as

$$\begin{aligned}\Delta P^{\mathrm{norm}} &= \Delta P_{\tau_{\mathrm{sf}}}^{\mathrm{norm}} + \Delta P_{\zeta}^{\mathrm{norm}} + \Delta P_{h_{\mathrm{B}}}^{\mathrm{norm}} + \Delta P_{\mathrm{ME,OOP}}^{\mathrm{norm}} + \Delta P_{\mathrm{ME,IP}}^{\mathrm{norm}} + \text{cross terms} \\ &\approx \frac{\gamma M_{\mathrm{s}}}{2\alpha\omega M_{\mathrm{LNO}} W}\left[\frac{C^2 M_{\mathrm{s}}^2\omega^2}{\gamma^2\omega_y^2}\left|\frac{J_{\mathrm{s}}^{\tau_{\mathrm{sf}}}}{u_0}\right|^2 + \frac{C^2 M_{\mathrm{s}}^2\omega^2}{\gamma^2\omega_y^2}\left|\frac{J_{\mathrm{s}}^{\zeta}}{u_0}\right|^2 + \left|\frac{h_{\mathrm{B}}}{u_0}\right|^2 + \frac{\omega^2}{\omega_y^2}\left|\frac{h_{\mathrm{ME}}^{\mathrm{OOP}}}{u_0}\right|^2 + \left|\frac{h_{\mathrm{ME}}^{\mathrm{IP}}}{u_0}\right|^2 + \text{cross terms}\right] \qquad (16) \\ &\approx A_0\left(\frac{\omega}{\omega_0}\right)^9 + B_0\left(\frac{\omega}{\omega_0}\right)^7 + C_0\left(\frac{\omega}{\omega_0}\right)^3 + D_0\left(\frac{\omega}{\omega_0}\right)^1 + \text{cross terms}, \qquad (17)\end{aligned}$$

where $\omega_y = \gamma M_{\mathrm{s}}/\mu_0$. The first, second, third, fourth, fifth, and sixth terms in Eq. (16) correspond to the contributions of $J_{\mathrm{s}}^{\tau_{\mathrm{sf}}}$, J_{s}^{ζ}, h_{B}, $h_{\mathrm{ME}}^{\mathrm{OOP}}$, $h_{\mathrm{ME}}^{\mathrm{IP}}$, and their products, respectively. Note that ΔP^{norm} in Eq. (16) is independent of u_0 because all contributions are proportional to u_0. By substituting Eqs. (3)–(6) in Eq. (16), one obtains Eq. (17) which shows the frequency dependence of ΔP^{norm} explicitly, where $\omega_0 = 2\pi \times 1.30$ GHz. The contributions of $J_{\mathrm{s}}^{\tau_{\mathrm{sf}}}$ and J_{s}^{ζ} are proportional to the ninth and seventh order of frequency, respectively, while h_{B} and $h_{\mathrm{ME}}^{\mathrm{OOP}}$, and $h_{\mathrm{ME}}^{\mathrm{IP}}$ lead to third- and first-order variation, respectively. From Fig. 5, we found that the slopes of the double-logarithmic plot were 7.4 and 6.8 for NiFe/Cu and NiFe/Pt bilayers, respectively, which implies that the SWR was excited by the STT from the SC proportional to ζ. On the other hand, the MW absorption in NiFe/Ti and NiFe showed the 4.0th- and 3.1th-power order of frequency, respectively, which is consistent with the frequency dependence of the power loss $\Delta P_{h_{\mathrm{B}}}^{\mathrm{norm}}$ owing to the Barnett effect. We also confirmed that the in-plane and out-of-plane ME fields excited the SWR in Ni because the slope of the double-logarithmic plot was between 1 and 3.

Finally, we discuss the material dependence of ζ. From the SWR intensity at 1.60 GHz for NiFe/Cu and NiFe/Pt bilayers, the amplitudes of the alternating SC injected to NiFe can be evaluated as 3.2×10^9 and 4.3×10^9 A m^{-2}, respectively. Here, the magnitude of the MW exciting the R-SAW was fixed at -5 dBm, and the values of u_0 were evaluated from the Barnett effect in the NiFe single layer [41]. From the evaluated SC amplitudes and Eqs. (3) and (4), the values of ζ for Cu and Pt were evaluated as 5.0×10^6 and 1.6×10^6, respectively. We also confirmed that a similar magnitude of ζ (2.6×10^6) was evaluated for Cu by an alternative method using a spin pumping effect in a R-SAW injected Pt/NiFe/Cu trilayer [42]. It is nontrivial that ζ values for Cu and Pt are comparable although the strengths of SOI are totally different between Cu and Pt. The result seems to imply that the microscopic SVC mechanism of angular momentum conversion with R-SAW is robust against the SOI which is one of the possible conversion mechanisms between spin and orbital angular momenta of electrons. Conversely, the generation of SC by dynamical lattice strain in metals with SOI at impurities has been also predicted theoretically [43]. We need both experimental and

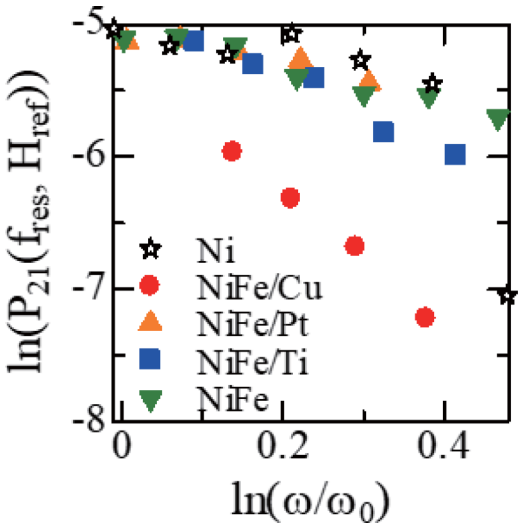

FIG. 6. Frequency dependence of $P_{21}(f_{\mathrm{ref}}, H_{\mathrm{ref}})$.

theoretical studies to understand the microscopic mechanism of the SVC, especially for the role of SOI.

VI. SUMMARY

In summary, we demonstrated highly nonlinear frequency-dependent SWR excited via SVC using an R-SAW. The MW absorption owing to the SWR excitation by the STT, the Barnett effect, and/or the ME effect can be distinguished from the difference in the frequency variations. From the comparison between Cu and Pt as a SC source, we found that the amplitudes of SC generated via SVC in R-SAW were similar between them, although Cu shows much weaker SOI than Pt. The finding will pave the way not only to fundamental understanding of the SC-generation mechanism via SVC but also to utilizing weak-SOI materials for spintronic devices.

ACKNOWLEDGMENTS

This work was partially supported by JST CREST Grant No. JPMJCR19J4, Japan, and JSPS KAKENHI Grant No. JP18H03867, and M.M. was partially supported by the Priority Program of Chinese Academy of Sciences Grant No. XDB28000000.

APPENDIX: FREQUENCY DEPENDENCE OF R-SAW AMPLITUDE

Figures 6 shows the frequency dependence of $P_{21}(f_{\mathrm{ref}}, H_{\mathrm{ref}})$ in the form of a double-logarithmic plot. As shown in Fig. 6, the peak intensity of the R-SAW decreases with increasing the frequency. Higher fundamental frequency of the R-SAW can be realized in narrower and denser IDTs because the wavelength of the R-SAW is determined by the structural period of the IDTs. The decrease in the electrode width leads to the increase in the electrical resistance of the IDT. As a consequence, the loss owing to the Joule heating of IDTs increases with increasing the fundamental frequency of the R-SAW as shown in Fig. 6.

As shown in Fig. 6, the peak intensity of the R-SAW transmitted through the NiFe/Cu bilayer was smaller than the others. The total thickness of the NiFe/Cu bilayer was one order of magnitude thicker than the others. The increase in the thickness of metallic thin films deposited between IDTs leads to a change in the acoustic impedance of the film. Thus, larger loss of the R-SAW transmission in the NiFe/Cu bilayer is attributable to the mismatch of the acoustic impedance between the film and $LiNbO_3$ substrate.

[1] H. Ohno, T. Endoh, T. Hanyu, N. Kasai, and S. Ikeda, IEDM Tech. Dig. 218 (2010).
[2] M. Hosomi, H. Yamagishi, T. Yamamoto, K. Bessho, Y. Higo, K. Yamane, H. Yamada, M. Shoji, H. Hachino, C. Fukumoto, H. Nagao, and H. Kano, IEDM Tech. Dig. 459 (2005).
[3] T. Kishi, H. Yoda, T. Kai, T. Nagase, E. Kitagawa, M. Yoshikawa, K. Nishiyama, T. Daibou, M. Nagamine, M. Amano, S. Takahashi, M. Nakayama, N. Shimomura, H. Aikawa, S. Ikegawa, S. Yuasa, K. Yakushiji, H. Kubota, A. Fukushima, M. Oogane, T. Miyazaki, and K. Ando, IEDM Tech. Dig. 309 (2008).
[4] S. Ikeda, J. Hayakawa, Y. M. Lee, F. Matsukura, Y. Ohno, T. Hanyu, and H. Ohno, IEEE Trans. Electron Devices **54**, 991 (2007).
[5] S. Matsunaga, J. Hayakawa, S. Ikeda, K. Miura, H. Hasegawa, T. Endoh, H. Ohno, and T. Hanyu, Appl. Phys. Express **1**, 091301 (2008).
[6] S. Kiselev, J. Sankey, I. Krivorotov, N. Emley, R. Schoelkopf, R. Buhrman, and D. Ralph, Nature (London) **425**, 380 (2003).
[7] W. H. Rippard, M. R. Pufall, S. Kaka, S. E. Russek, and T. J. Silva, Phys. Rev. Lett. **92**, 027201 (2004).
[8] J. A. Katine and E. E. Fullerton, J. Magn. Magn. Mater. **320**, 1217 (2008).
[9] K. Uchida, S. Takahashi, K. Harii, J. Ieda, W. Koshibae, K. Ando, S. Maekawa, and E. Saitoh, Nature (London) **455**, 778 (2008).
[10] F. J. Jedema, A. T. Filip, and B. J. van Wees, Nature (London) **410**, 345 (2001).
[11] E. Saitoh, M. Ueda, H. Miyajima, and G. Tatara, Appl. Phys. Lett. **88**, 182509 (2006).
[12] K. Uchida, H. Adachi, T. An, T. Ota, M. Toda, B. Hillebrands, S. Maekawa, and E. Saitoh, Nat. Mater. **10**, 737 (2011).
[13] K. Uchida, T. An, K. Kajiwara, M. Toda, and E. Saitoh, Appl. Phys. Lett. **99**, 212501 (2011).
[14] K. Uchida, H. Adachi, T. An, H. Nakayama, M. Toda, B. Hillebrands, S. Maekawa, and E. Saitoh, J. Appl. Phys. **111**, 053903 (2012).
[15] Y. K. Kato, R. C. Myers, A. C. Gossard, and D. D. Awschalom, Science **306**, 1910 (2004).
[16] J. Wunderlich, B. Kaestner, J. Sinova, and T. Jungwirth, Phys. Rev. Lett. **94**, 047204 (2005).
[17] T. Kimura, Y. Otani, T. Sato, S. Takahashi, and S. Maekawa, Phys. Rev. Lett. **98**, 156601 (2007).
[18] J. C. Rojas Sánchez, L. Vila, G. Desfonds, S. Gambarelli, J. P. Attané, J. M. De Teresa, C. Magén, and A. Fert, Nat. Commun. **4**, 2944 (2013).

[19] K. Shen, G. Vignale, and R. Raimondi, Phys. Rev. Lett. **112**, 096601 (2014).
[20] M. Matsuo, J. Ieda, K. Harii, E. Saitoh, and S. Maekawa, Phys. Rev. B **87**, 180402(R) (2013).
[21] R. Takahashi, M. Matsuo, M. Ono, K. Harii, H. Chudo, S. Okayasu, J. Ieda, S. Takahashi, S. Maekawa, and E. Saitoh, Nat. Phys. **12**, 52 (2015).
[22] D. Kobayashi, T. Yoshikawa, M. Matsuo, R. Iguchi, S. Maekawa, E. Saitoh, and Y. Nozaki, Phys. Rev. Lett **119**, 077202 (2017).
[23] G. Okano, M. Matsuo, Y. Ohnuma, S. Maekawa, and Y. Nozaki, Phys. Rev. Lett. **122**, 217701 (2019).
[24] C. G. de Oliverira and J. Tiomno, Nuovo Cimento **24**, 672 (1962).
[25] B. Mashhoon, Phys. Rev. Lett. **61**, 2639 (1988).
[26] J. Anandan, Phys. Rev. Lett. **68**, 3809 (1992).
[27] B. Mashhoon, Phys. Rev. Lett. **68**, 3812 (1992).
[28] F. W. Hehl and W.-T. Ni, Phys. Rev. D **42**, 2045 (1990).
[29] S. J. Barnett, Phys. Rev. **6**, 239 (1915).
[30] H. Chudo, M. Ono, K. Harii, M. Matsuo, J. Ieda, R. Haruki, S. Okayasu, S. Maekawa, H. Yasuoka, and E. Saitoh, Appl. Phys. Express **7**, 063004 (2014).
[31] M. Ono, H. Chudo, K. Harii, S. Okayasu, M. Matsuo, J. Ieda, R. Takahashi, S. Maekawa, and E. Saitoh, Phys. Rev. B **92**, 174424 (2015).
[32] M. Imai, Y. Ogata, H. Chudo, M. Ono, K. Harii, M. Matsuo, Y. Ohnuma, S. Maekawa, and E. Saitoh, Appl. Phys. Lett. **113**, 052402 (2018).
[33] M. Weiler, L. Dreher, C. Heeg, H. Huebl, R. Gross, M. S. Brandt, and S. T. B. Goennenwein, Phys. Rev. Lett. **106**, 117601 (2011).
[34] L. Dreher, M. Weiler, M. Pernpeintner, H. Huebl, R. Gross, M. S. Brandt, and S. T. B. Goennenwein, Phys. Rev. B **86**, 134415 (2012).
[35] M. Matsuo, Y. Ohnuma, and S. Maekawa, Phys. Rev. B **96**, 020401(R) (2017).
[36] L. D. Landau and E. M. Lifshitz, *Theory of Elasticity* (Pergamon, New York, 1959).
[37] J. C. Slonczewski, J. Magn. Magn. Mater. **159**, L1 (1996).
[38] K. Y. Guslienko, R. W. Chantrell, and A. N. Slavin, Phys. Rev. B **68**, 024422 (2003).
[39] R. Sasaki, Y. Nii, Y. Iguchi, and Y. Onose, Phys. Rev. B **95**, 020407(R) (2017).
[40] W. Robbins, IEEE Trans. Sonics Ultrason. **24**, 339 (1977).
[41] Y. Kurimune, M. Matsuo, and Y. Nozaki, Phys. Rev. Lett. **124**, 217205 (2020).
[42] S. Tateno, G. Okano, M. Matsuo, and Y. Nozaki, Phys. Rev. B **102**, 104406 (2020).
[43] T. Funato and H. Kohno, J. Phys. Soc. Jpn. **87**, 073706 (2018).